ACS Sustainable Chemistry & Engineering

Research Article

pubs.acs.org/journal/ascecg

Green Nanocomposites Based on Functionalized Cellulose Nanocrystals: A Study on the Relationship between Interfacial Interaction and Property Enhancement

Hou-Yong Yu,*[,†,‡,§] Zong-Yi Qin,[‡] Chen-Feng Yan,[†] and Ju-Ming Yao*[,†,§]

[†]The Key Laboratory of Advanced Textile Materials and Manufacturing Technology of Ministry of Education, College of Materials and Textile, Zhejiang Sci-Tech University, Hangzhou 310018, China

[‡]State Key Laboratory for Modification of Chemical Fibers and Polymer Materials, College of Materials Science and Engineering, Donghua University, Shanghai 201620, China

[§]National Engineering Lab of Textile Fiber Materials & Processing Technology, Zhejiang Sci-Tech University, Hangzhou 310018, China

Supporting Information

ABSTRACT: Functionalized cellulose nanocrystals (PHCNs) were synthesized by grafting poly(3-hydroxybutyrate-co-3-hydroxyvalerate) (PHBV) onto cellulose nanocrystals (CNCs). The resultant PHCNs with high loading levels were uniformly dispersed into a PHBV matrix to produce fully biodegradable nanocomposites, which showed superior mechanical performance and thermal stability. Compared with those of neat PHBV, the tensile strength, Young's modulus, and elongation at break of the nanocomposites with 20 wt % PHCNs were enhanced by 113%, 95%, and 17%, respectively. Meanwhile, the initial decomposition temperature (T_0), temperature at 5% weight loss ($T_{5\%}$), maximum decomposition temperature (T_{max}), and complete decomposition temperature (T_f) increased by 29.6, 23.9, 34.7, and 37.0 °C, respectively. This improvement was primarily ascribed to uniform dispersion of the PHCNs and to strong interfacial adhesion between filler and matrix due to the chain entanglements, cocrystallization, and hydrogen bonding interactions. Moreover, the nanocomposites showed a wider melt-processing window than neat PHBV. Furthermore, the crystallinity and hydrophilic properties of the nanocomposites could be modulated through with the increase of the PHCN contents. In addition, the nanocomposites were nontoxic to human MG-63 cells. Such high performance bionanocomposites have great potential in expanding the utilization of CNCs from natural resources and practical application as PHBV-based bioplastic and biomedical materials.

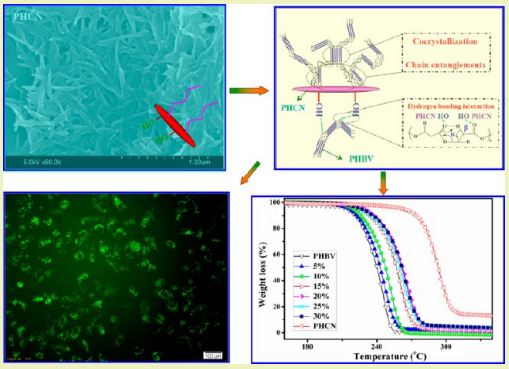

KEYWORDS: *Cellulose nanocrystals, Poly(3-hydroxybutyrate-co-3-hydroxyvalerate), Bionanocomposite, Interfacial interaction, Mechanical property, Thermal stability*

INTRODUCTION

It is well-known that the poor mechanical and thermal properties of biodegradable polymers (poly(3-hydroxybutyrate-co-3-hydroxyvalerate), polylactic acid, polycaprolactone) always restrict their wide applications as eco-friendly and biomedical materials. So intense efforts have been made to develop novel green nanocomposites based on biodegradable polymers and renewable polysaccharide materials (cellulose, starch, and chitin), because these nanocomposites could replace some petrochemical polymers and overcome serious "white pollution".[1−6] Especially, cellulose nanocrystals (CNCs) extracted from natural cellulose materials can act as reinforcing agents to reinforce many biodegradable polymeric matrices, such as poly(3-hydroxybutyrate-co-3-hydroxyvalerate) (PHBV),[7−10] polylactic acid (PLA),[11−14] polycaprolactone (PCL),[2,15−19] poly(propylene carbonate) (PPC),[4] and alginate.[20] However, the hydrophilic nature and abundant hydroxyl groups of the CNCs make them difficult disperse into common nonpolar solvents or hydrophobic matrix and thus CNCs often aggregate easily, leading to poor compatibility between the CNCs and hydrophobic polymer matrix. Hence, low reinforcement efficiency of CNCs in the nanocomposites occurred due to a poor nanocrystal−matrix interface as the weakest point.[4,16] In order to prevent the CNCs from aggregating and to improve their dispersion and the compatibility within the matrix material, addition of compatibilizer or surfactant and using a template method based on solvent exchange are employed.[4,7,8,10,21,22] However, compatibilizers were intended to interact with nanofillers or matrix, which would inhibit the formation of hydrogen bonding interactions between the reinforcing phase and matrix.[8] Additionally, surfactants with high contents are needed for the high surface area of CNCs and cause the thermal degradation of matrix polymers.[4,11,13]

Received: November 28, 2013
Revised: January 9, 2014
Published: January 13, 2014

Scheme 1. Schematic Diagram of Synthesis Routes of PHCN Copolymer

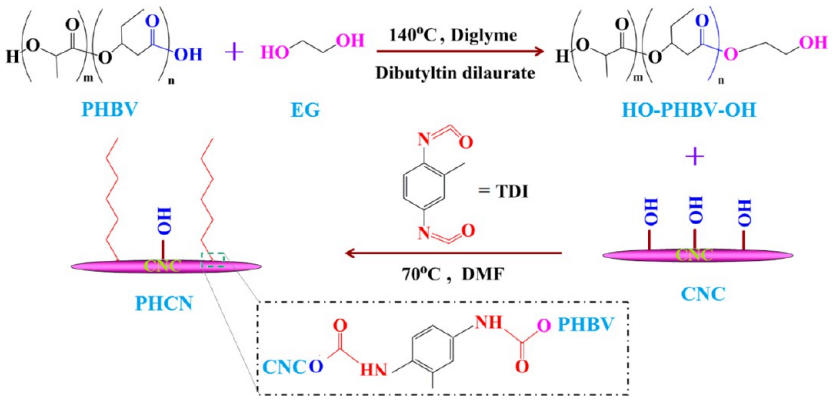

Further, the solvent exchange process during the template preparation was complicated and time-consuming due to repeated successive centrifugation steps.[7,10,21] We[7,10] and other groups[8] previously reported on reinforcing PHBV systems with different types of CNCs and observed a significant stiffness increase at filler contents in the range of 1−10 wt %. However, an obvious decrease in elongation at break of the nanocomposites occurred, and the CNC loading levels were usually lower than 10 wt % due to poor interfacial compatibility.

Recently, graft polymerization as a simple and powerful technique of CNC surface modification can prevent their aggregations due to covalent linkage between the CNCs and hydrophobic polymers[2,12,15−19] or low molecular weight esters.[11,13,22] Especially, grafting polymer chains on CNC surfaces can also act as reinforcing fillers and efficient compatibilizers in the nanocomposites without consideration of the miscibility between two components when the grafted polymer chains and the matrix are the same. Therefore, the strong interfacial adhesion can be achieved by formation of a continuous interphase between the modified CNC phase and polymer matrix phase. More recently, cellulose nanocrystals-*graft*-poly(3-hydroxybutyrate-co-3-hydroxyvalerate) copolymers (PHCNs) with various lengths and grafting density of PHBV side chains were successfully prepared in our laboratory, and the obtained PHCNs with improved hydrophobicity can be easily dispersed in various kinds of solvents.[23] In the present work, in order to improve the dispersion and compatibility of CNCs within PHBV matrix, the thermally stable PHCNs with higher grafting density of long side chains were introduced to PHBV matrix to prepare green bionanocomposites via a simple solution casting method, in which the entanglements (and cocrystallization) between grafted PHBV side chains and polymer matrix chains were expected to occur. To the best of our knowledge, there is no evidence to simultaneously investigate the effect of the chain entanglements, cocrystallization, and hydrogen bonding interactions of functionalized CNCs and the PHBV matrix on the crystallization behavior and properties of the nanocomposites. Therefore, in order to obtain the relationship between the interfacial interaction of PHCNs within PHBV and final properties of the nanocomposites, the influence of the PHCNs with different contents on microstructure, crystallization behavior, and mechanical, thermal, and hydrophobic properties of the highly filled nanocomposites was investigated. Moreover, comparative cytocompatibility of neat PHBV and PHBV/PHCN nanocomposites were also studied with human MG-63 cells for the potential biomedical application.

EXPERIMENTAL SECTION

Materials. PHBV with 2.57 mol % 3-hydroxyvalerate (HV) (M_n = 5.90 × 10^4, M_w = 1.58 × 10^5) was obtained from Tiannan Biological Material Co., Ltd. (Ningbo, China) and purified by reprecipitation in methanol from chloroform solutions. Commercial microcrystalline celluloses (MCCs, particle size: about 20 μm), toluene diisocyanate (TDI), ethanol (99.8%), diglyme, *N*,*N*-dimethyl formamide (DMF), chloroform, ethylene glycol (EG), dibutyltin dilaurate (90.0%), hydrochloric acid (HCl), ammonia solution ($NH_3.H_2O$), petroleum ether, and phosphate buffered solution (PBS) were purchased from the Shanghai Guoyao Group Chemical Reagent Co., Ltd. (Shanghai, China). The human MG-63 cells, an osteosarcoma cell line, were purchased from Shanghai Institute of Biochemistry and Cell Biology. Fetal bovine serum (FBS) and Dulbecco's modified Eagle's medium (DMEM) were obtained from Gibco (USA). The Cell Counting Kit-8 was purchased from Beyotime Institute of Biotechnology (China). The Actin-Tracker Green was purchased from Biyuntian Biology Technology Co., Ltd. All other chemicals were of analytical grade and purchased from Hangzhou Mike Chemical Agents Company (China). All reagents and solvents were used as received or purified using standard procedures.

Extraction of Cellulose Nanocrystals. The details for preparing the cellulose nanocrystals (CNCs) have been given elsewhere.[24] The aqueous CNC suspension was prepared by HCl hydrolysis of the MCCs in the hydrothermal kettle at 110 °C for 3 h. The residual HCl in the CNC suspension was neutralized by 3 M ammonia solution at room temperature ($NH_4OH + HCl \rightarrow NH_4Cl + H_2O$). The sublimation of NH_4Cl took place at 100 °C for 1 h, so the ammonium groups can be removed. After 10 min of exposure to ultrasonic irradiation, the CNC suspension was freeze-dried for 48 h to obtain the dry CNCs. Moreover, the dry CNCs were Soxhlet extracted using ethanol to remove adsorbed organic compounds before use.[25]

Synthesis of PHCN Copolymers. Telechelic OH-terminated PHBV oligomers (denoted as HO−PHBV−OH) were prepared by a transesterification procedure as our previously reported method[26,27] (Scheme 1). The detailed synthesis process was as follows: 30 g PHBV and 300 mL of diglyme were placed in a flask and, then, the flask was heated to 140 °C in an oil bath with continuously mechanical stirring under nitrogen atmosphere. After PHBV was dissolved completely, 60 mL of ethylene glycol and dibutyltin dilaurate (0.3 g) as catalyst were added into the flask. After 7.5 h, the products were precipitated with ethanol, washed repeatedly with ethanol, and dried under vacuum. The molecular weight of the resulting OH-terminated PHBV oligomers was about 1980 g mol^{-1} by measurement with gel permeation chromatography.[26,27]

Grafting OH-terminated PHBV oligomers onto the surface of CNCs was carried out through the condensation reaction by using toluene diisocyanate (TDI) as coupling agent as previously reported method[26,27] (Scheme 1). The detailed synthesis process was as follows: 1.0 g CNC and 80 mL of anhydrous DMF were added into a 250 mL four-neck flask with a mechanical stirrer, nitrogen inlet, and outlet.

dx.doi.org/10.1021/sc400499g | ACS Sustainable Chem. Eng. 2014, 2, 875−886

Then the flask was heated to 120 °C in an oil bath with mechanical stirring. After any trace water of the stirred mixture was removed until only 50 mL of DMF remained in the flask. Then the flask was cooled to 70 °C, some TDI (2.467 g) and ten drops of dibutyltin dilaurate were sequentially added into the flask for 1 h under a nitrogen atmosphere. Subsequently, 4.0 g PHBV oligomers were added into the flask with continuous mechanical stirring. After a desired reaction time of 48 h, the resulting products were redissolved into chloroform to remove the cross-linked substances and, then, precipitated by using a mixture of anhydrous alcohol and petroleum ether twice to remove the catalyst. Finally, the ungrafted PHBV oligomers were removed by using Soxhlet extractor. The product was wrapped by a filter paper and, then, soaked in the chloroform (as extracting agent). Then, the ungrafted PHBV was removed after reflux condenser with chloroform for 12 h. The pure copolymer was finally dried at 40 °C under vacuum overnight and designated as PHCN. The tested films for static contact angle test were prepared by dissolving the copolymer in chloroform (10 wt %).

Preparation of the PHBV/PHCN Nanocomposites. PHBV/PHCN nanocomposites (5−30 wt % PHCNs) were prepared by gradually adding the PHCN into chloroform solution of PHBV in ice water bath for 30 min under ultrasonic irradiation. Then the PHBV/PHCN nanocomposite films with the thickness of approximately 50 μm were obtained on a glass slide through solution casting technique. After being visibly dried, the films were further dried under vacuum at 40 °C until no obvious absorption of chloroform (754 cm^{-1}) appeared in the IR spectrum.

Cell Culture Assay, Morphology, and Attachment. The human MG-63 cells, an osteosarcoma cell line, were maintained in Dulbecco's modified Eagle's medium (DMEM) with 10% fetal calf serum (FCS) and antibiotics (100 U mL^{-1} penicillin, 100 U mL^{-1} streptomycin) at 37 °C and in a 5% CO_2 atmosphere. MG-63 cells were digested using 0.25% trypsin for about 1 min and resuspended in the medium. Cell numbers were determined by counting via a haemacytometer, and then diluted to the concentration of 1×10^5 cells mL^{-1}. All the nanocomposite films were disinfected with 75% ethanol and washed with phosphate buffered solution (PBS), three times. Then the samples were placed into the 24-well cell culture plates, followed by adding 1 mL cell suspension to each well.

After the MG-63 cells were cultured for 2 h, the culture medium with unattached cells was carefully removed from the wells by a pipet. All the nanocomposite films were then washed with PBS buffer. Subsequently, the MG-63 cells were identified by Actin-Tracker Green, which allowed the measurement of the cytoplasmic area and consequent estimation of cellular spreading. The fluorescence images were photographed by a fluorescence microscope (Olympus IX71-22FL/PH). The cell initial attachment was evaluated after the cultivation for 2 h. The cell culture medium was discarded and the samples were washed with PBS buffer for three times. The attached cells were stained with Actin-Tracker Green and were qualitatively using fluorescence microscopy. A mean value for three places of each sample was determined. A Cell Count Kit-8 (CCK-8) was employed to quantitatively evaluate the cell attachment in different composites according to the instruction of CCK-8. The OD values (absorbance) were measured in a microplate reader at 450 nm. The data reported were the mean of three examinations.

Characterization. The ^{1}H NMR spectra of PHBV oligomers and the resulting copolymers were obtained from a Bruker Avance 400 NMR spectrometer in 5 mm tubes with $CDCl_3$ as a solvent at room temperature. The optical properties of neat PHBV and the nanocomposite films were characterized on a UV−vis spectrophotometer (Hitachi U-2900, Japan) in the wavelength interval between 200 and 900 nm. The morphologies of CNC, PHCN, and fracture morphologies of the nanocomposite films were observed on a field emission scanning electron microscopy (FE-SEM, HITACHI S-4800) at 5.0 kV. The films were frozen in liquid nitrogen and fractured. FT-IR spectra were recorded on a Nicolet 8700 FT-IR spectrophotometer. Pellets of dried CNCs, PHCNs, PHBV, and the nanocomposite films were made with KBr. Each spectrum was collected with 64 scans and 2 cm^{-1} resolution at room temperature. Wide-angle XRD measurements (WAXD) were carried out on a RIGAKU D/Max-2550 PC diffractometer with an area detector operating under Cu Kα (1.5418 Å) radiation (40 kV, 40 mA) at room temperature. All the samples were kept for 2 weeks at room temperature to reach equilibrium crystallization before measuring. The degree of crystallinity was taken as the ratio of the sum of areas under the crystalline diffraction peaks to the total area under the curve between $2\theta = 10$ and 60°. The crystallite sizes of 002 lattice planes were estimated by using the well-known Scherrer equation:[9,10]

$$D_{hkl} = \frac{0.9\lambda}{B_{hkl} \cos \theta} \quad (1)$$

where D_{hkl} is the crystallite size in the direction normal to the hkl family of lattice planes, λ is the radiation wavelength (1.54 Å), and B_{hkl} is the full width at half−maximum in radians of the reflection of that family of lattice planes.

DSC measurements of neat PHBV and the nanocomposite films were performed on MDSC TA-2910 differential scanning calorimeter by employing a 40 mL min^{-1}, flow of dry nitrogen as a purge gas for the sample and reference cells. The sample was first heated from room temperature to 200 °C at a rate of 20 °C/min and kept at 200 °C for 5 min to eliminate the previous heat history. Subsequently, the sample was cooled to −50 °C at a rate of 10 °C/min and heated again to 200 °C at a rate of 10 °C/min. The main thermal parameters were obtained from DSC curves, such as melt crystallization temperature (T_{mc}), melt crystallization enthalpies (ΔH_{mc}), cold crystallization temperature (T_{cc}), cold crystallization enthalpies (ΔH_{cc}), melting temperature (T_{m1}, T_{m2}, T_{m3}), and melting enthalpies (ΔH_m).

Tensile properties of neat PHBV and the nanocomposite films were measured on a Kexin WDW3020 electronic universal testing machine. Tensile specimens with about 10 mm in width, about 50 μm in thickness, and 50 mm in gauge length were loaded at a constant tensile rate of 1 mm/min, and ten replicates were tested for each sample. The thickness of films was modulated by using solution-casting apparatus with thickness adjustment when the solution of nanocomposites was homogeneous.

TGA was carried out using Netzsch TG209 F1 TGA instrument coupled with QMS. The samples were heated at 10 °C min^{-1} from room temperature to 600 °C in a dynamic nitrogen atmosphere with the flow rate of 30 mL min^{-1}.

The contact angles of the neat PHBV, PHCN, and the nanocomposite films were measured on the air surface of their films using pendant drop method on a Dataphysics OCA40 contact angle analyzer at room temperature. About 2 μL of deionized water was dropped onto the surface at a contact time of 5 s. Twenty independent determinations at different sites of the sample were averaged.

RESULTS AND DISCUSSION

Optical Property. The nanocomposite films with various PHCN contents were visually examined for qualitative differences in transparency and external appearance as shown in the photograph (Figure 1). The nanocomposite films maintained the transparency of neat PHBV. With the increase of PHCN contents, the transparency was progressively lost while the agglomeration phenomenon of the PHCNs within the PHBV matrix could be observed (PHCN contents exceeded to 25 wt %). It suggests that the PHCNs had good dispersion within the PHBV matrix so that the nanocomposites were free from light scattering. Further, the UV−vis transmittance spectra of neat PHBV and the nanocomposite films at visible wavelength range of 400−800 nm are shown in Figure 1. There was an initial slight decrease in transmittance at low PHCN loading followed by a sharp decrease at higher loading. With the increase of the PHCN contents, the transmittance decreased from 91% for neat PHBV to 50% for the nanocomposite with 30 wt % PHCNs. This decrease in transmittance may be due to the formation of fewer agglomerates in the nanocomposite films with high loading levels. From above, it indicated that less than 20 wt % PHCNs had good compatibility with polymer matrix to avoid the nanofiller aggregation and to reduce the number of light scatters, as a result, the relatively high

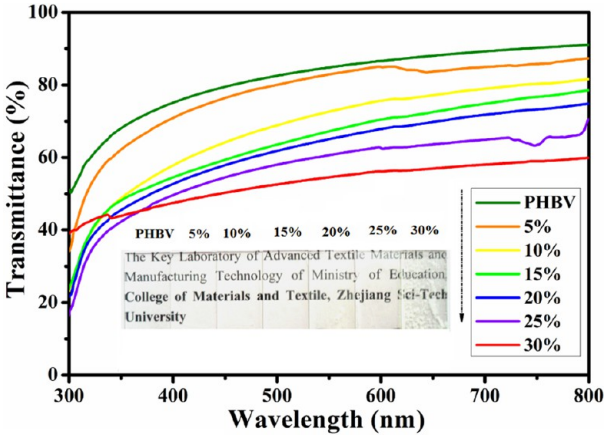

Figure 1. UV−vis transmittance spectra for neat PHBV and the nanocomposites with various PHCN contents (the insets give photographs of the samples).

transmittance of the visible light through the nanocomposites could be kept.

Fractured Morphology. FE-SEM was used to investigate morphological changes of the CNCs associated with the surface graft copolymerization. As shown in Figure 2, the FE-SEM image showed that the ungrafted CNCs with rodlike morphology were about 20 nm in diameter and 200−300 nm in length, the aspect ratio was about 12.5, as was also found in our previous report.[24] After surface grafting PHBV onto CNCs, it seemed that the rodlike shape of PHCNs was preserved, but its size was slightly increased. The average diameter and length were 30 and 315 nm, respectively. Thus its aspect ratio was 10.5. In addition, the outline of the PHCN was blurry, which may be resulted from partial solubilization of the cellulose molecules after graft copolymerization.[23] Moreover, the nanocrystals were less individualized than native ones and were believed to aggregate because the presence of hydrophobic PHBV chains on the nanocrystal likely triggered the CNC aggregation upon drying.

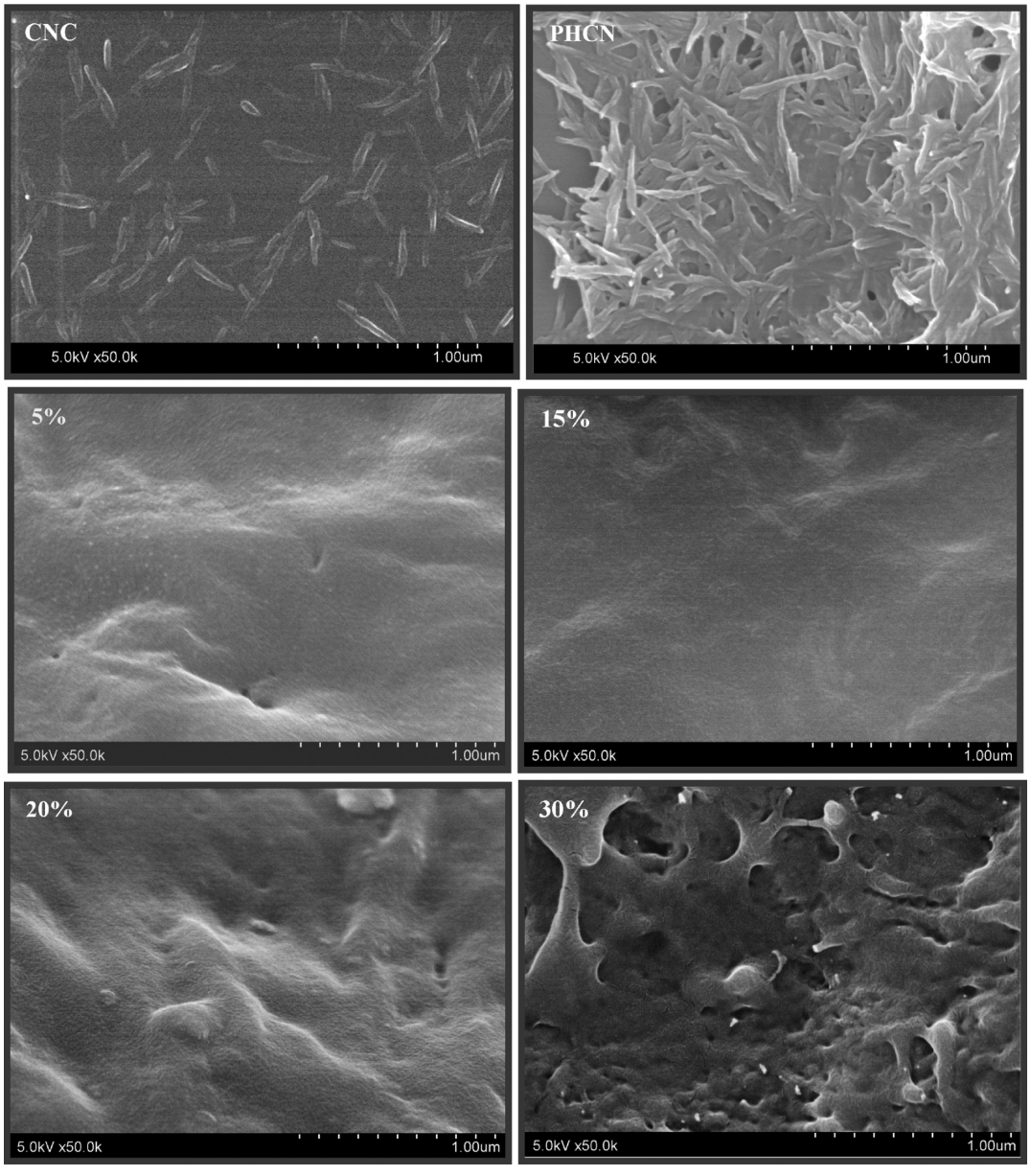

Figure 2. FE-SEM images for the CNCs, PHCNs, and the fractured morphologies of the nanocomposites with the PHCN contents of 5, 15, 20, and 30 wt %.

To evaluate the dispersion of the PHCNs within PHBV, FE-SEM observations for the fractured morphologies of the PHBV/PHCN nanocomposites were investigated and the fractographs were shown in Figure 2. When PHCN content was below 15 wt %, similar striated and smooth fractured surface was observed for both the nanocomposites, meanwhile no rod-like PHCN was found in the nanocomposites, which indicated PHCNs were well embedded into the matrix, suggesting a rather good dispersion of PHCNs within the PHBV matrix and strong interfacial interaction between two components. When the PHCN content was 20 wt %, a few bumps appeared on the fracture surface of nanocomposites, but these bumps were also well-embedded into the matrix. This indicated that PHCNs with high loading levels still exhibited good miscibility with PHBV matrix. However, with a continuous increase of PHCN contents (higher than 20 wt %), some large conglomerations and cavities were observed, which was attributed to self-aggregation of the superfluous PHCNs.

Chemical Structure. FT-IR spectra of neat PHBV, PHCNs, and the nanocomposites with various PHCN contents are shown in Figure 3. Compared to neat PHBV, three new bands at 3348, 1660, and 1542 cm^{-1} assigned to the symmetric stretching vibration and medium bending vibration of N−H from imino group (−OOCNH−) of polyurethane linkage appeared in the PHCNs. This implied PHCNs were successfully prepared by using toluene diisocyanate (TDI) as the coupling agent. At the same time, the peaks at 1602 and 1453 cm^{-1} were related to aromatic groups of TDI.[23] Moreover, from ^1H NMR spectra (Supporting Information Figure S1), compared to OH-terminated PHBV oligomer, new peaks at 1.12 and 7.00 ppm, and multiple peaks around 2.86−2.95 ppm belonged to the protons of methyl group and the benzene ring, −NH−COO from TDI, indicating that the PHCN copolymer was successfully prepared. The degree of polymerization of PHBV (DP), the degree of substitution of copolymer (DS), and the number average molecular weight of the grafted PHBV segments in the copolymer were 32.5, 0.72, and 46332.0 g mol^{-1}, respectively (in Supporting Information Table S1). Further, CNC fractions in the PHCN (ϕ_{CNC}) were about 22%.

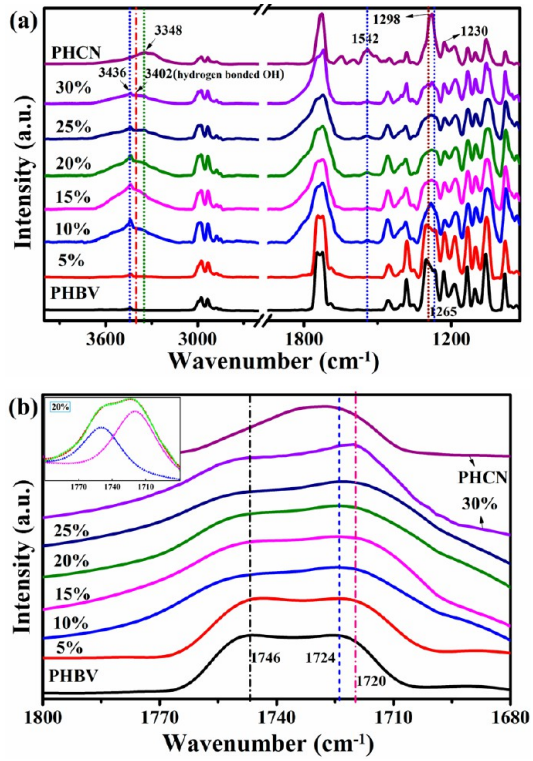

Figure 3. FT-IR spectra (a) and carbonyl stretching region ($\nu_{C=O}$) in the infrared spectra (b) for neat PHBV, PHCN, and the nanocomposites with various PHCN contents and peak deconvolution for the nanocomposites with 20 wt % PHCNs (inset).

In addition, the peaks at 1542 cm^{-1} appeared in FT-IR spectra of the nanocomposites, indicating the presence of PHCNs in the nanocomposites. Besides that, compared to the PHCNs, Two typical O−H stretching bands at 3402 and 3436 cm^{-1} appeared in the FT-IR spectra of the nanocomposites, which were ascribed to the stretching vibrations of the hydrogen bonded and free O−H groups, respectively.[7−10] With the increase of PHCN contents from 0 to 20 wt.%, the intensity for the hydrogen bonded O−H band increased, whereas for the free O−H band slightly decreased. When the PHCN contents continued to increase, the intensity for the hydrogen bonded O−H band decreased. From above, it showed that no new chemical bonds appeared in the nanocomposites, but the strong hydrogen bonding between the residual hydroxyl groups of PHCNs as proton donors and carbonyl bands of PHBV as proton acceptors did occur.

In order to investigate the influence of hydrogen bonding interaction on crystallization of the nanocomposites, the crystallization sensitive bands of PHBV were classified. For example, the bands at 1453 and 1381, 1298 and 1265, and 1230 cm^{-1} were attributed to CH_2 shear vibration peak, CH_2—CO stretching vibration, and CH_2 bending vibration, respectively.[28−32] Then the intensity of carbonyl group (C═O) stretching vibration peak was normalized, the intensity of crystallization sensitive bands peak was compared with the increase of the PHCN contents, which can be used to determine the crystalline components in the nanocomposites. As shown in Figure 3a, it is found that with the increase of PHCN contents, the intensity of IR peaks at 1265 and 1381 cm^{-1} became weak; meanwhile, the intensity of the other crystallization sensitive bands was also reduced significantly. This indicated that, by adding the PHCNs, the crystalline components in the nanocomposites were decreased due to different crystallization rate and thus chain entanglement between PHBV matrix chains and PHBV side chains from PHCNs.

To determine the hydrogen bond fraction (F_{H-CO}), IR spectra of the carbonyl band in the range from 1680 and 1800 cm^{-1} were curve-fitted by using Gauss/Lorentz spectral function. As shown by the insert presented in Figure 3b, the band situated at around 1720 cm^{-1} can be assigned to the hydrogen bonded C═O groups, and 1746 cm^{-1} to free C═O groups.[7,10,33] It was observed that with the increase of the PHCN contents, compared to neat PHBV, the band position for hydrogen-bonded component decreased to 1720 cm^{-1} for all the nanocomposites. This was ascribed to intermolecular hydrogen bonding interaction between PHCN residual hydroxyl groups and PHBV carbonyl groups, weakening the polarity of carbonyl groups and thus resulting in the decrease in the position of the C═O band.[10] However, the area of the hydrogen-bonded C═O bands became larger, and then slightly decreased. So F_{H-CO} values were determined to further analyze the change of hydrogen bonding interaction in the nanocomposites, which can be calculated by the following equation:[7,10,33,34]

$$F_{H-CO} = \frac{A_H/r_{H/a}}{(A_H/r_{H/a} + A_a)} \quad (2)$$

dx.doi.org/10.1021/sc400499g | ACS Sustainable Chem. Eng. 2014, 2, 875−886

Table 1. Hydrogen Bond Fractions (F_{H-CO}), Crystallinities (X_c), and Thermal Parameters of Nonisothermal Crystallization and Melting Behaviors of Neat PHBV, PHCNs, and the Nanocomposites with Various PHCN Contents

sample	F_{H-CO}[a]	X_c (%)[b]	D_{002} (nm)[b]	T_g (°C)[c]	T_{mc} (°C)[c]	ΔH_{mc} (J/g)[c]	T_{cc} (°C)[c]	T_{m1} (°C)[c]	T_{m2} (°C)[c]	T_{m3} (°C)[c]	ΔH_m (J/g)[c]
PHBV		58.1	30.9	−19.3			32.8	92.8	114.2	130.0	74.7
5%	0.15	56.3	28.3	−16.9			33.2	90.5	112.2	129.6	68.8
10%	0.18	54.8	26.0	−14.9			36.7	89.7	112.2	130.0	66.5
15%	0.25	53.2	25.1	−13.7			38.8	95.6	117.3	132.4	64.3
20%	0.29	51.0	23.5	−12.1			39.1	99.5	121.3	136.7	61.6
25%	0.26	51.8	23.8	−9.0			44.5	101.5	122.1	136.8	62.3
30%	0.25	52.7	23.9	−6.6			45.0	108.3	128.4	139.1	63.5
PHCN		55.5	20.2		77.9	56.7		136.5	150.8		65.8

[a]Hydrogen bond fractions (F_{H-CO}) was obtained from deconvoluted FT-IR spectra. [b]Crystallinities (X_c) and crystallite size (D_{002}) values were calculated from the WAXD patterns. [c]Glass transition temperature (T_g), melt crystallization temperature (T_{mc}), melt crystallization enthalpies (ΔH_{mc}), cold crystallization temperature (T_{cc}), cold crystallization enthalpies (ΔH_{cc}), melting temperature (T_{m1}, T_{m2}, T_{m3}), and melting enthalpies (ΔH_m) were obtained from DSC curves.

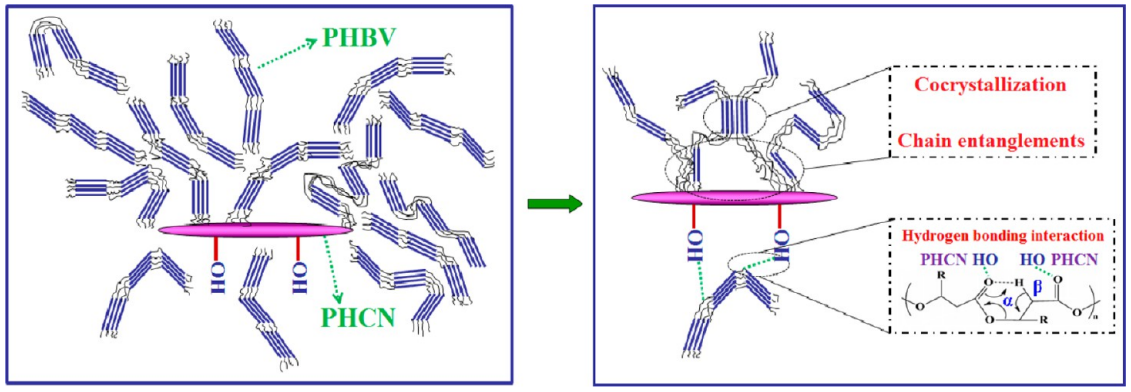

Figure 4. Sketch for the formation of hydrogen bonding interaction and evolution of polymer aggregation structure and crystal structure in the PHBV/PHCN nanocomposites.

where A_a and A_H are the peak areas of free and hydrogen bonded component, respectively, and $r_{H/a}$ is the specific absorption ratio of the above two bands. For semiquantitative comparison purposes, $r_{H/a}$ should be within a range from 1.2 to 1.75, depending on the strength of the hydrogen bonds. Herein a minimal error would be obtained by using 1.35 of $r_{H/a}$, being close to 1.32 applied for PHBV/CNC nanocomposites.[7,10] Table 1 presents the F_{H-CO} of the nanocomposites as a function of the PHCN contents. With the increase of the PHCN contents, F_{H-CO} first increased from 0.15 to a maximum value of 0.29 for 20 wt %, and then slightly decreased to 0.25 for 30 wt %. From above, it is clearly seen that among all the nanocomposites, the strongest intermolecular interaction appeared in the nanocomposite with 20 wt % PHCNs due to good dispersion within the polymer matrix, as presented schematically in Figure 4. Generally, good dispersion of PHCN and thus intermolecular interaction formation were beneficial to simultaneously improve mechanical and thermal properties of the nanocomposites.[7,10] In addition, it should be noted that the F_{H-CO} of the PHBV/PHCN nanocomposites was lower than that for the PHBV/CNC nanocomposites (0.37, 10 wt % CNCs).[7] It could be explained that more hydroxyl groups of CNCs from PHCN were substituted by copolymerization with PHBV side chains, and thus amounts of formed hydrogen bonding interactions were reduced.

Crystal Structure. WAXD was used to study the crystal structure of neat PHBV, PHCNs, and the nanocomposites with various PHCN contents. In Supporting Information Figure S2, the (110) plane of the nanocomposites was heavily overlapped by the (200) plane of CNCs and the (110) plane of PHBV. As shown in Figure 5, all the characteristic diffraction peaks of

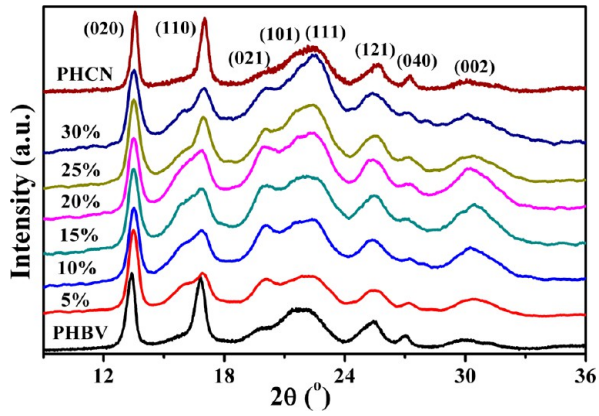

Figure 5. WAXD patterns of neat PHBV, PHCNs and the nanocomposites with various PHCN contents.

PHBV and PHCNs appeared in the diffraction patterns of the nanocomposites, suggesting that the crystal structure of PHBV was essentially maintained even the introduction of PHCN. However, compared to neat PHBV, an obvious decrease in the intensity for the (110) plane of the nanocomposites was observed, and accompanied by appearance of a shoulder (15.9°). It indicated that the crystal growth of PHBV was limited in the (110) plane, but its preferential growth in other crystal planes occurred, such as (021) and (002) plane. Further, when the PHCN contents increased from 0 to 20 wt %, the intensities for the (021) and (002) plane were obviously increased. When less than 20 wt % PHCNs were added into the PHBV matrix, one end

dx.doi.org/10.1021/sc400499g | ACS Sustainable Chem. Eng. 2014, 2, 875−886

of the PHBV macromolecular chains was fixed due to chain entanglements and intermolecular hydrogen bonding interaction between two components. Therefore, chain movement of PHBV became easier along the vertical direction of the rodlike PHCNs. When PHCN contents exceeded to 25 wt %, a decrease in the intensity of the two planes occurred, indicating that the agglomeration of PHCNs within the PHBV matrix would restrict the preferential growth of PHBV crystals. Similar phenomena also appeared in the PCL/clay and PHBV/montmorillonite (MMT) nanocomposites.[35,36] Besides that, compared to neat PHBV, the width at half-height of the diffraction peak became broad, indicating that PHBV crystals in the nanocomposites showed the smaller size. Table 1 lists the crystallinity (X_c) of neat PHBV, PHCN, and the nanocomposites. The nanocomposites showed lower crystallinity than neat PHBV. With the increase of PHCN contents, the X_c first decreased from the 58.1% (PHBV) to 51.0% (20 wt % PHCNs) and, then, increased gradually to 52.7% (30 wt % PHCNs). This is because PHBV crystallization would be hindered by chain entanglement and hydrogen bonding interactions (in Figure 4), which can result in the formation of more imperfect PHBV crystals and thus reduce its crystallinity. However, PHCN with higher contents weakened strong interaction with the polymer matrix due to its agglomeration, leading to slight increase in crystallinity of the nanocomposites. In addition, the D_{002} of the nanocomposite was smaller than that of neat PHBV and decreased dramatically with the increase of PHCN contents, indicating that PHCNs hindered the diffusion and folding of PHBV chains due to the confinement effects of the PHCNs. Especially, the nanocomposites with 20 wt % PHCNs exhibited the smallest D_{002} among all the nanocompostes, hinting that the strongest confinement effects occurred in the nanocomposites due to homogeneous dispersion of PHCNs within PHBV (meaning large interfacial areas between PHCNs and PHBV or the formation of chain entanglement and hydrogen bonding interactions) as revealed by FE-SEM observations (in Figure 2). Similar phenomenon was found in CNC/PHBV nanocomposites reported by Ten et al.[9] and our group.[10] In general, the refined crystal structures could contribute to improved mechanical properties of the nanocomposites.

Crystallization and Melting Behavior. The crystallinity plays an important role in the physical properties and biodegradability of biodegradable polymers. Therefore, the crystallization behavior of the nanocomposites was investigated. Figure 6 shows the DSC curves of neat PHBV, PHCN, and the nanocomposites with various PHCN contents during first cooling and second heating processes, and the corresponding thermal parameters are listed in Table 1. As shown in Figure 6a, a strong crystallization peak at 77.9 °C was observed for PHCN; however, no obvious melt crystallization peaks of neat PHBV and the nanocomposites were observed during the first cooling scans, but the cold crystallization peaks can be found during the second heating scans. This indicated that the crystallization ability of PHBV was not improved by adding PHCN, and probably cocrystallization of grafted PHBV chains on the CNC surfaces with PHBV matrix chains occurred. The glass transition temperature (T_g) was measured to judge the chain entanglements between polymer matrix and reinforcing materials.[37−40] Generally, when the chain entanglements is formed, the glass transition temperature tends to increase.[39,40] Figure 6b clearly shows that compared to neat PHBV, the T_g of the nanocomposites were increased gradually with increase of PHCN contents. This could be explained that the hydrogen bonding interactions and chain entanglements restricted the segmental motion of PHBV

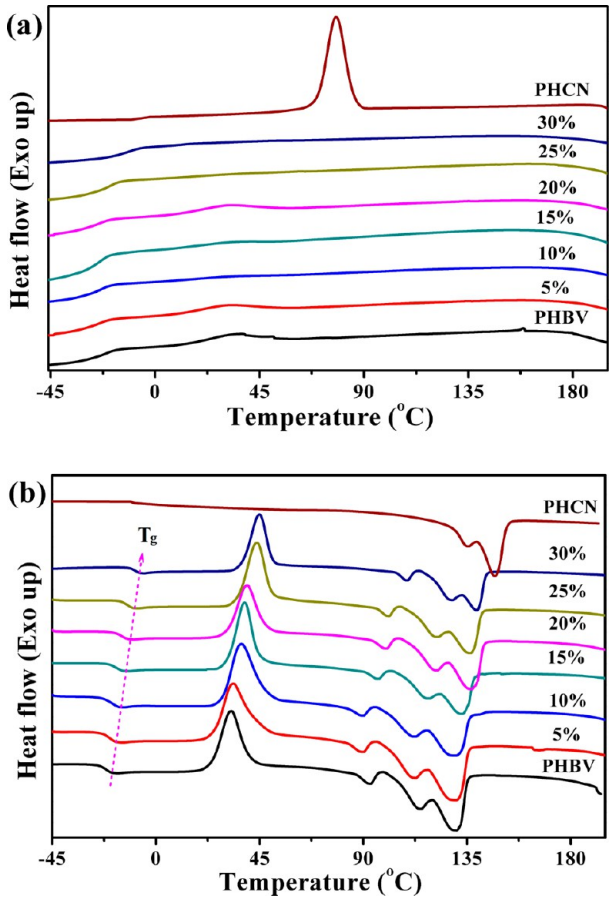

Figure 6. DSC curves of neat PHBV, PHCNs, and the nanocomposites with various PHCN contents: (a) the first cooling scan; (b) the second heating scan.

polymer chains, leading to enhancement on the stiffness of PHBV chains. A similar trend was found in the cold crystallization temperature of the nanocomposites, which indicated that the crystallization of PHBV was becoming more difficult because strong chain entanglement between two components would be formed with increase of PHCN contents. When the nanocomposites absorbed enough energy to break the chain entanglements, the crystalline chains in the nanocomposites would refold and recrystallize.

Generally, the second heating trace was used to measure the crystal structure formed during the nonisothermal crystallization. Therefore, the melting behavior of neat PHBV, PHCN, and the nanocomposites during the second heating processes was illustrated in Figure 6b. Neat PHBV and all the nanocomposites exhibited triple melting peaks (T_{m1}, T_{m2}, and T_{m3}), whereas double melting peaks appeared in the PHCNs. A weak single melting peak in the range of 90−109 °C (T_{m1}) was observed, which might be caused by the melt of the imperfect PHBV crystals. Furthermore, the samples showed a double melting peak at two higher nearby temperatures (T_{m2} and T_{m3}), which could be due to melting−recrystallization−melting process of PHBV crystals.[3,7−10,26,28] This means that the second endothermic peak (T_{m2}) should be used as the melting temperature of the nanocomposites. When PHCN content was below 10 wt %, the nanocomposite showed lower melting temperature than neat PHBV (114.2 °C), which was due to the occurrence of chain entanglement between PHCN and PHBV matrix, resulting in the imperfect crystals and thus decrease of melting point. When the

dx.doi.org/10.1021/sc400499g | ACS Sustainable Chem. Eng. 2014, 2, 875−886

PHCN contents exceeded 10 wt %, The melting temperature increased from 112.2 °C (10 wt %) to 128.4 °C (30 wt %). This could be attributed to the contribution of PHCN with the higher melting temperature (compared to neat PHBV). In addition, with the increase of the PHCN contents, the width at half-height of the third endothermic peak (T_{m3}) was almost increased, which indicated that due to strong chain entanglement, less content of recrystallized component was formed after melting, leading to smaller width at half-height. With the increase of the PHCN contents, the crystallinity obtained from DSC curves (X_{DSC}) first decreased to minimum value for the nanocomposite with 20 wt % PHCNs, and then, increased (Supporting Information Table S2). This result was in agreement with FT-IR and WAXD results.

Mechanical Properties. Figure 7 gives the tensile strength, Young's modulus, and elongation to break as a function of PHCN contents for neat PHBV and the PHBV/PHCN nanocomposites. It is clear that a strong reinforcement effect in the mechanical properties of the nanocomposite films was achieved by adding PHCN into PHBV matrix. When the PHCN contents increased from 0 to 20 wt %, the tensile strength, Young's modulus, and elongation at break were increased greatly. This suggests that a strong adhesion between the reinforcing phase and the matrix existed in the nanocomposites, resulting in an efficient dispersion of the PHCNs and efficient stress transfer at the interface. When PHCN contents were 20 wt %, the best mechanical property of the nanocomposites could be achieved. The tensile strength and Young's modulus were improved by 113 and 95%, respectively,

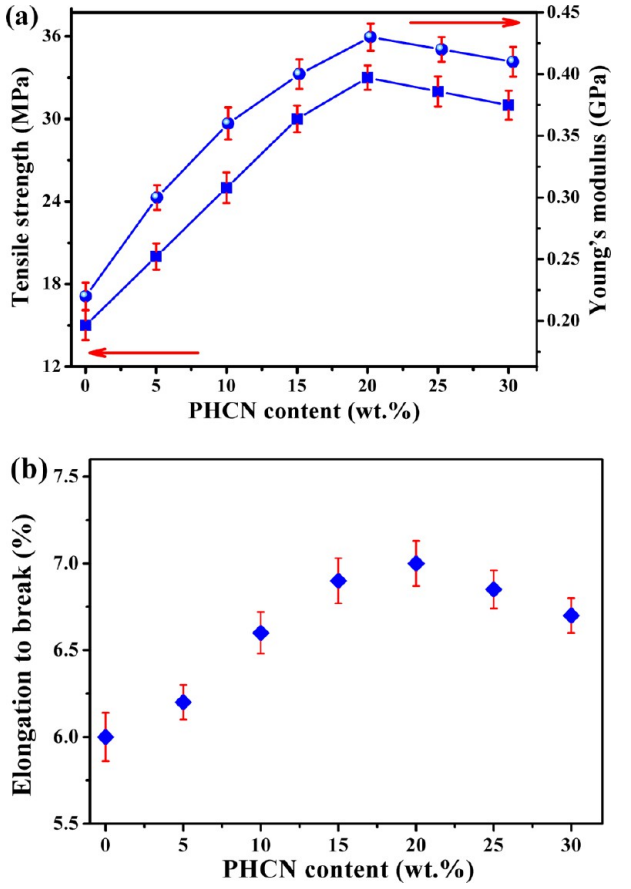

Figure 7. Tensile strength and Young's modulus (a) and elongation to break (b) as a function of PHCN contents for neat PHBV and the PHBV/PHCN nanocomposites.

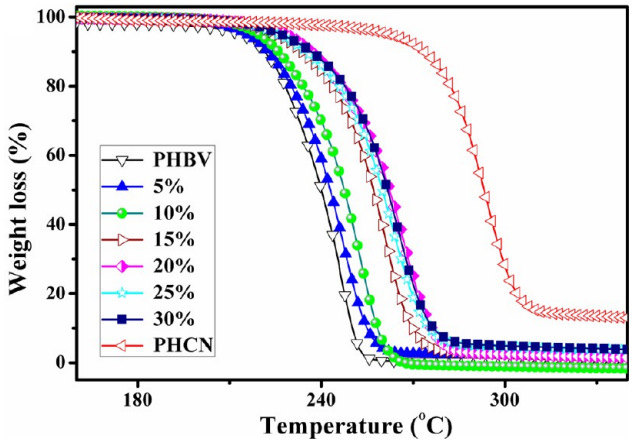

Figure 8. TGA curves for neat PHBV, PHCNs, and the nanocomposites with various PHCN contents.

Table 2. Thermal Analysis Parameters for Neat PHBV, PHCN, and the Nanocomposites with Various PHCN Contents

sample	T_0 (°C)[a]	$T_{5\%}$ (°C)[a]	T_{max} (°C)[a]	T_f (°C)[a]	T_0-T_{m3} (°C)[b]
PHBV	229.4	216.8	245.8	252.3	99.4
5%	234.5	219.9	252.6	261.2	104.9
10%	240.4	223.7	259.2	266.9	110.4
15%	254.3	236.7	272.2	281.2	121.9
20%	259.0	240.7	279.5	289.3	122.3
25%	254.6	237.8	273.4	284.2	117.8
30%	256.6	238.5	275.4	285.6	117.5
PHCN	279.5	231.9	294.1	303.5	/

[a]The initial decomposition temperature (T_0), temperature at 5% weight loss ($T_{5\%}$), maximum decomposition temperature (T_{max}), and complete decomposition temperature (T_f) were obtained from the TGA curves at the heating rate of 10 °C/min. [b]T_0-T_{m3} stood for the melt-processing window.

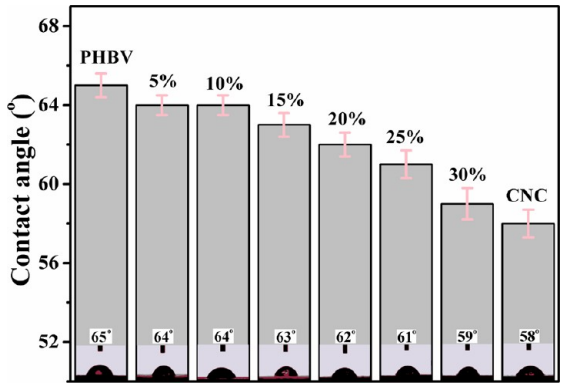

Figure 9. Contact angles of neat PHBV, PHCN, and the nanocomposites with various PHCN contents.

and elongation at break was also increased by 17%. These improvements could be attributed to the restrained chain movement and refined crystalline structure during the deformation due to chain entanglements and hydrogen bonding interactions because the PHCNs with PHBV side chains were easily dispersed into PHBV matrix. Similar enhancement in PCL matrix was achieved due to the formation of strong chain entanglements and cocrystallization between polymer matrix and poly(ε-caprolactone)-grafted cellulose nanocrystals.[15,16] However, once the PHCN contents

dx.doi.org/10.1021/sc400499g | ACS Sustainable Chem. Eng. 2014, 2, 875−886

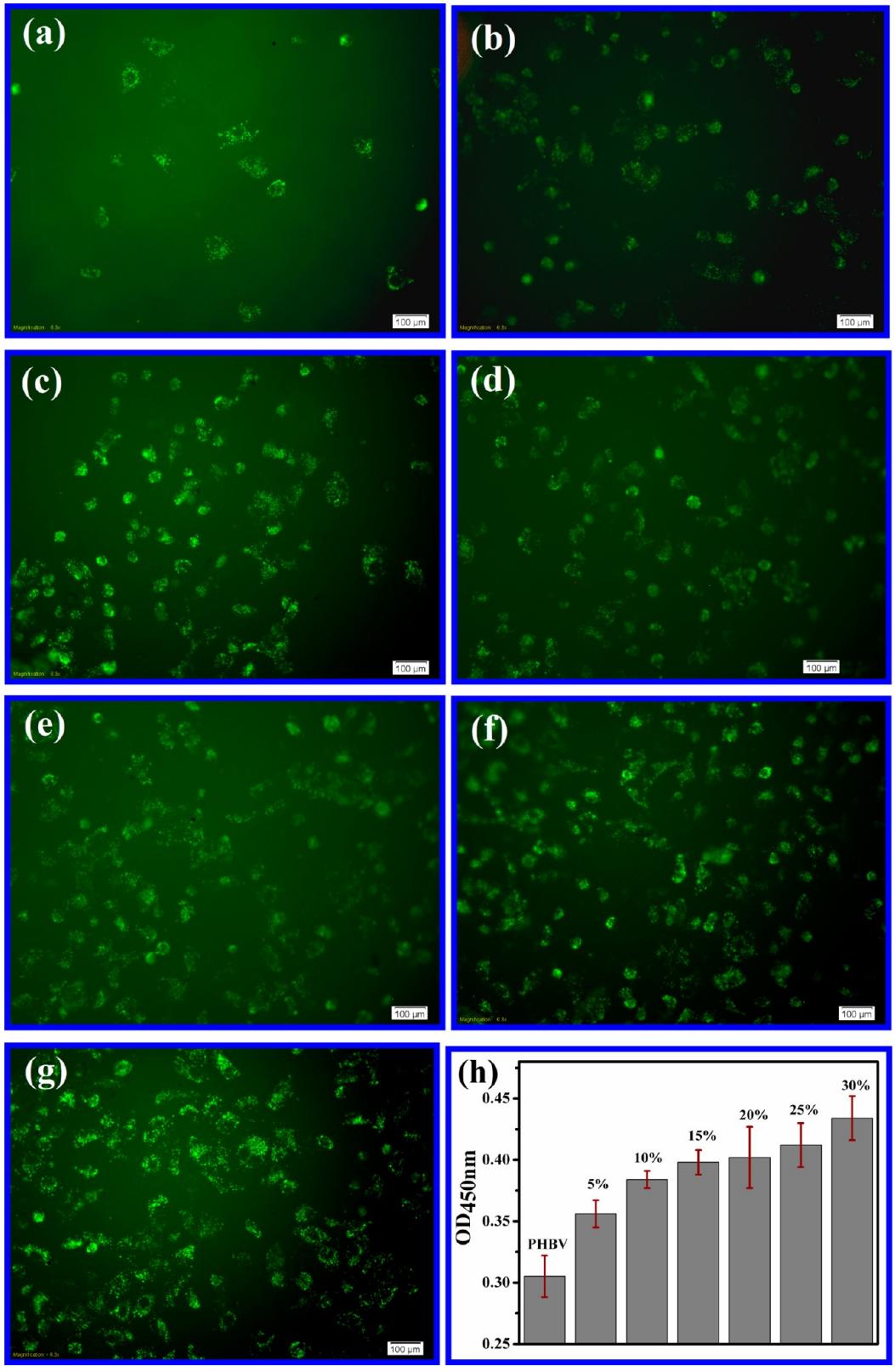

Figure 10. Fluorescence microscopy images of neat PHBV (a) and the nanocomposite films with various PHCN contents [(b) 5%, (c) 10%, (d) 15%, (e) 20%, (f) 25%, (g) 30%], and (h) CCK-8 assays of MG-63 attachment.

exceeded 20 wt %, slight decreases in the tensile strength, Young's modulus, and the elongation to break occurred because of slight PHCN agglomeration, which could be supported by the FE-SEM observations. In addition, Voigt upper bound and Reuss lower bound models were used to discuss the experimental results of the tensile properties.[41] With the addition of PHCNs, the great improvement was also within the upper and lower bound models (in Supporting Information Table S2).

Thermal Stability. Figure 8 shows the TGA curves of neat PHBV, PHCN, and the nanocomposites at the heating rate of 10 °C/min, and the main thermal parameters are summarized in Table 2. Thermal degradation through a one-step process was observed, and the thermal stability of the nanocomposites was better than neat PHBV (245.6 °C). This result can be ascribed to the formation of hydrogen bonding interactions between ester carbonyl groups of PHBV chains and hydroxyl groups of PHCNs, which would decrease the electron-donating effect of substituent group of carbon atoms at α-position and negative inductive effect of the neighboring group of methylene group at the β-position to the ester oxygen of PHBV matrix.[7,28] As a result, hydrogen bonding interactions could suppress the formation of six-membered ring ester during the degradation process of PHBV (in Figure 4) and, thus, enhance its thermal stability. However, the thermal decomposition temperature of the nanocomposites was lower than that of neat PHCNs (294.1 °C), which was ascribed to poor crystallization ability and the formation of imperfect crystals.

As shown in Table 2, with the increase of the PHCN contents, the maximum decomposition temperature (T_{max}) gradually increased from 245.8 °C for neat PHBV to the maximum of 279.5 °C for the nanocomposite with 20 wt % PHCNs and then decreased slightly to 275.4 °C for 30 wt % PHCNs. The similar trend was also observed for initial decomposition temperature (T_0), temperature at 5% weight loss ($T_{5\%}$), and complete decomposition temperature (T_f). Compared with those for neat PHBV, the T_0, $T_{5\%}$, T_{max}, and T_f for the nanocomposites with the best thermal stability increase by about 29.6, 23.9, 34.7, and 37.0 °C, respectively. Such enhancement can be attributed to the strongest chain entanglements and hydrogen bonding interactions, which was consistent with FT-IR and DSC results. In addition, the T_0-T_{m3} values of neat PHBV and the nanocomposites were calculated and listed in Table 2, which could reflect the melt-processing window. Generally, the larger the T_0-T_{m3} value of the polymer, the wider the melt-processing window.[27] As shown in Table 2, the T_0-T_{m3} value of the nanocomposites was higher than that for neat PHBV, illustrating the nanocomposites exhibited the wider melt-processing window. Moreover, among all the nanocomposites, the nanocomposites with 20 wt % PHCNs showed the widest melt-processing window.

Hydrophilic Property. The crystallinity and hydrophilicity are the important factors to affect the cell biocompatibility (cell adhesion and growth) on the surfaces of biodegradable materials.[26,42,43] Lowering the crystallinity and augmenting the hydrophilicity of cellulose-based materials are well-known approaches to improve their biodegradability in vivo for biomedical materials.[26,42] Static contact angle measurements were used to estimate the hydrophilicity of neat PHBV, PHCN, and the nanocomposites films as shown in Figure 9. It can be observed that all the nanocomposites have lower contact angle than 65° for neat PHBV, which can be attributed to the change of microstructure in the nanocomposites, such as the ratio of the crystalline components and the bumps in the films. This agrees with the results of the FE-SEM. However, with the increase of the PHCN contents, the contact angle of the nanocomposites gradually decreased from 64° to 59°, which might be ascribed to addition of relatively hydrophilic PHCNs with lower contact angle of 58°.

Cytocompatibility. The human MG-63 used were cultured on films composed of neat PHBV and PHBV/PHCN nanocomposites with PHCN contents of 5−30 wt % to assess the basic cytocompatibility of these materials and to evaluate their potential applications for biomaterials. The image of fluorescent and the OD values were used for the qualitative and quantitative attachment analyses of MG-63 on neat PHBV and the nanocomposite films, respectively. As shown in Figure 10a−g, cells cultured on the nanocomposite films were obviously more numerous than those for neat PHBV film. With the increase of PHCN contents, cells (stained green) on the nanocomposite films were increased greatly. This was attributed to the increased hydrophilicity of the nanocomposite films, promoting cells attachment on the surface of films. Results of CCK-8 assay in Figure 10h shows that the OD values of the nanocomposites were significantly higher than that of neat PHBV film. As the PHCN contents increased, the OD values increased greatly. These results implied that the addition of PHCNs (functionalized CNCs) could effectively improve cell−matrix interactions by providing more binding sites for MG-63 cell adhesion. Indeed, Mahmoud et al. had found that surface structure of functionalized CNCs played an important role in cellular uptake and cytotoxicity.[44] From above, it indicated that such nanocomposites possessed excellent biocompatibility and had a wide potential in biomedical application.

CONCLUSIONS

Rodlike PHCNs were successfully prepared and used to process green nanocomposites by a solution casting method using PHBV as matrix. It is found that highly filled PHCN was uniformly dispersed into PHBV matrix when the PHCN content was below 20 wt %. Simultaneous enhancements on the mechanical property and thermal stability of green nanocomposites were achieved. Compared with those of PHBV, the tensile strength, Young's modulus, and elongation at break of the nanocomposites with 20 wt % PHCNs were improved by 113%, 95%, and 17%, respectively. At the same time, the T_0, $T_{5\%}$, T_{max}, and T_f increased by 29.6, 23.9, 34.7, and 37.0 °C, respectively. This was mainly attributed to the endurance of higher stress of the PHCNs and the interfacial adhesion between fillers and matrix thanks to chain entanglements, cocrystallization, and hydrogen bonding interactions. The nanocomposites also exhibited a wider melt-processing window than neat PHBV. Moreover, the improved hydrophilic properties and good biocompatibility in MG-63 cells, and decreased crystallinity of the nanocomposites, could be achieved by introducing PHCN with different loading levels. These PHBV/PHCN nanocomposite films can be considered as potential biomedical materials and green plastics as replacements for traditional petrochemical plastics.

ASSOCIATED CONTENT

Supporting Information

^{1}H NMR spectra of the grafting parameters, CNC fractions in the PHCN (ϕ_{CNC}), structure parameters, and number average molecular weight of the grafted PHBV segments in the PHCN copolymer; FT-IR spectra and WAXD patterns of neat PHBV, CNCs, PHCNs, and the nanocomposites with 20 wt % PHCNs; crystallinity (X_{DSC}), Young's modulus (E_Y), longitudinal modulus (E_L), and transverse modulus (E_T) for neat PHBV, PHCN, and the nanocomposites with various PHCN contents. This material is available free of charge via the Internet at http://pubs.acs.org.

AUTHOR INFORMATION

Corresponding Authors

*Tel.: 86 571 86843618. Fax: 86 571 86843619. E-mail address: yaoj@zstu.edu.cn (J.-M.Y.).
*E-mail address: phdyu@zstu.edu.cn (H.-Y.Y.).

Notes

The authors declare no competing financial interest.

ACKNOWLEDGMENTS

This work was supported by the National Natural Science Foundation of China (51172207), The Young Researchers Foundation of Key Laboratory of Advanced Textile Materials and Manufacturing Technology, Ministry of Education, Zhejiang Sci-Tech University (2013QN06), and Top Priority Discipline of Zhejiang Province in Zhejiang Sci-Tech University (2013YBZX01), Program for Department of Education of Zhejiang Province (Y201327880), the Scientific Research Foundation of Zhejiang Sci-Tech University (ZSTU) under Grant. No. 13012115-Y, and the Natural Science Foundation of Zhejiang Province of China (LQ12C16005).

REFERENCES

(1) Park, S. H.; Oh, K. W.; Kim, S. H. Reinforcement effect of cellulose nanowhisker on bio−based polyurethane. *Compos. Sci. Technol.* **2013**, *86*, 82−88.

(2) Chen, G.; Dufresne, A.; Huang, J.; Chang, P. R. A Novel Thermoformable Bionanocomposite Based on Cellulose Nanocrystal-graft-Poly(ε-caprolactone). *Macromol. Mater. Eng.* **2009**, *294*, 59−67.

(3) Wang, J.; Wang, Z.; Li, J.; Wang, B.; Liu, J.; Chen, P.; Miao, M.; Gu, Q. Chitin nanocrystals grafted with poly(3−hydroxybutyrate−co−3−hydroxyvalerate) and their effects on thermal behavior of PHBV. *Carbohydr. Polym.* **2012**, *87*, 784−789.

(4) Wang, D.; Yu, J.; Zhang, J.; He, J.; Zhang, J. Transparent bionanocomposites with improved properties from poly(propylene carbonate) (PPC) and cellulose nanowhiskers (CNWs). *Compos. Sci. Technol.* **2013**, *85*, 83−89.

(5) Habibi, Y.; Lucia, L. A.; Rojas, O. J. Cellulose nanocrystals: chemistry, self−assembly, and applications. *Chem. Rev.* **2010**, *110*, 3479−3500.

(6) Salam, A.; Lucia, L. A.; Jameel, H. A novel cellulose nanocrystals−based approach to improve the mechanical properties of recycled paper. *ACS. Sustainable. Chem. Eng.* **2013**, DOI: dx.doi.org/10.1021/sc400226m.

(7) Yu, H. Y.; Qin, Z. Y.; Liu, Y. N.; Chen, L.; Liu, N.; Zhou, Z. Simultaneous improvement of mechanical properties and thermal stability of bacterial polyester by cellulose nanocrystals. *Carbohydr. Polym.* **2012**, *89*, 971−978.

(8) Ten, E.; Turtle, J.; Bahr, D.; Jiang, L.; Wolcott, M. Thermal and mechanical properties of poly(3-hydroxybutyrate-co-3-hydroxyvalerate)/cellulose nanowhiskers composites. *Polymer* **2010**, *5*, 2652−2660.

(9) Ten, E.; Jiang, L.; Wolcott, M. P. Preparation and properties of aligned poly(3-hydroxybutyrate-co-3-hydroxyvalerate)/cellulose nanowhiskers composites. *Carbohydr. Polym.* **2012**, *90*, 541−550.

(10) Yu, H. Y.; Qin, Z. Y.; Liu, L.; Yang, X. G.; Zhou, Y.; Yao, J. M. Comparison of the reinforcing effects for cellulose nanocrystals obtained by sulfuric and hydrochloric acid hydrolysis on the mechanical and thermal properties of bacterial polyester. *Compos. Sci. Technol.* **2013**, *87*, 22−28.

(11) Pei, A.; Zhou, Q.; Berglund, L. A. Functionalized cellulose nanocrystals as biobased nucleation agents in poly (L−lactide)-(PLLA)−Crystallization and mechanical property effects. *Compos. Sci. Technol.* **2010**, *70*, 815−821.

(12) Lin, N.; Huang, J.; Chang, P. R.; Feng, J.; Yu, J. Surface acetylation of cellulose nanocrystal and its reinforcing function in poly(lactic acid). *Carbohydr. Polym.* **2011**, *83*, 1834−1842.

(13) Petersson, L.; Kvien, I.; Oksman, K. Structure and thermal properties of poly(lactic acid)/cellulose whiskers nanocomposite materials. *Compos. Sci. Technol.* **2007**, *67*, 2535−2544.

(14) Goffin, A. L.; Habibi, Y.; Raquez, J. M.; Dubois, P. Polyester−grafted cellulose nanowhiskers: A new approach for tuning the microstructure of immiscible polyester blends. *ACS Appl. Mater. Interfaces* **2012**, *4*, 3364−3371.

(15) Habibi, Y.; Dufresne, A. Highly filled bionanocomposites from functionalized polysaccharide nanocrystals. *Biomacromolecules* **2008**, *9*, 1974−1980.

(16) Habibi, Y.; Goffin, A. L.; Schiltz, N.; Duquesne, E.; Dubois, P.; Dufresne, A. Bionanocomposites based on poly(ε−caprolactone)−grafted cellulose nanocrystals by ring opening polymerization. *J. Mater. Chem.* **2008**, *18*, 5002−5010.

(17) Lönnberg, H.; Fogelström, L.; Azizi-Samir, M. A. S. L. B.; Malmström, E.; Hult, A. Surface grafting of microfibrillated cellulose with poly(ε−caprolactone)−Synthesis and characterization. *Eur. Polym. J.* **2008**, *44*, 2991−2997.

(18) Lönnberg, H.; Fogelström, L.; Zhou, Q.; Hult, A.; Berglund, L.; Malmström, E. Investigation of the graft length impact on the interfacial toughness in a cellulose/poly(ε−caprolactone) bilayer laminate. *Compos. Sci. Technol.* **2011**, *71*, 9−12.

(19) Zoppe, J. O.; Peresin, M. S.; Habibi, Y.; Venditti, R. A.; Rojas, O. J. Reinforcing poly (ε−caprolactone) nanofibers with cellulose nanocrystals. *ACS Appl. Mater. Interfaces* **2009**, *1*, 1996−2004.

(20) Lin, N.; Bruzzese, C.; Dufresne, A. tempo-oxidized nanocellulose participating as crosslinking aid for alginate−based sponges. *ACS Appl. Mater. Interfaces* **2012**, *4*, 4948−4959.

(21) Capadona, J. R.; Bergm, D. O. V.; Capadona, L. A.; Schroeter, M.; Rowan, D S. J.; Tyler, J.; Weder, C. A versatile approach for the processing of polymer nanocomposites with self-assembled nanofibre templates. *Nat. Nanotechnol.* **2007**, *2*, 765−769.

(22) Rueda, L.; d'Arlas, B. F.; Zhou, Q.; Berglund, L. A.; Corcuera, M. A.; Mondragon, I.; Eceiza, A. Isocyanate−rich cellulose nanocrystals and their selective insertion in elastomeric polyurethane. *Compos. Sci. Technol.* **2011**, *71*, 1953−1960.

(23) Yu, H. Y.; Qin, Z. Y. Surface grafting of cellulose nanocrystals with poly(3-hydroxybutyrate-co-3-hydroxyvalerate). *Carbohydr. Polym.* **2014**, *101*, 471−478.

(24) Yu, H. Y.; Qin, Z. Y.; Liang, B. L.; Liu, N.; Zhoun, Z.; Chen, L. Facile extraction of thermally stable cellulose nanocrystals with a high yield of 93% through hydrochloric acid hydrolysis under hydrothermal conditions. *J. Mater. Chem. A* **2013**, *1*, 3938−3944.

(25) Labet, M.; Thielemans, W. Improving the reproducibility of chemical reactions on the surface of cellulose nanocrystals: ROP of e-caprolactone as a case study. *Cellulose* **2011**, *18*, 607−617.

(26) Yu, H. Y.; Qin, Z. Y.; Wang, L. F.; Zhou, Z. Crystallization behavior and thermal properties of biodegradable ethyl cellulose-g-poly(3-hydroxybutyrate-co-3-hydroxyvalerate): The influence of the length and grafting density of the crystallizing side chains. *Carbohydr. Polym.* **2012**, *87*, 2447−2454.

(27) Yu, H. Y.; Yao, J. M.; Qin, Z. Y.; Liu, L.; Yang, X. G. Comparison of covalent and noncovalent interactions of carbon nanotubes on the crystallization behavior and thermal properties of poly(3-hydroxybutyrate-co-3-hydroxyvalerate). *J. Appl. Polym. Sci.* **2013**, *130*, 4299−4307.

(28) Liu, Q. S.; Zhu, M. F.; Wu, W. H.; Qin, Z. Y. Reducing the formation of six-membered ring ester during thermal degradation of biodegradable PHBV to enhance its thermal stability. *Polym. Degrad. Stab.* **2009**, *94*, 18−24.

(29) Fei, B.; Chen, C.; Wu, H.; Peng, S.; Wang, X.; Dong, L.; Xin, J. H. Modified poly(3-hydroxybutyrate-co-3-hydroxyvalerate) using hydrogen bonding monomers. *Polymer* **2004**, *45*, 6275−6284.

(30) Lao, H. K.; Renard, E.; Linossier, I.; Langlois, V.; Vallée-Rehel, K. Modification of poly(3-hydroxybutyrate-co-3-hydroxyvalerate) film by chemical graft copolymerization. *Biomacromolecules* **2007**, *8*, 416−423.

(31) Izumi, C. M. S.; Temperini, M. A. FT-Raman investigation of biodegradable polymers: Poly(3-hydroxybutyrate) and poly(3-hydroxybutyrate-co-3-hydroxyvalerate). *Vib. Spectrosc.* **2010**, *54*, 127−132.

(32) Cheng, M. L.; Sun, Y. M.; Chen, H.; Jean, Y. C. Change of structure and free volume properties of semi−crystalline poly(3-hydroxybutyrate-co-3-hydroxyvalerate) during thermal treatments by positron annihilation lifetime. *Polymer* **2009**, *50*, 1957−1964.
(33) Fei, B.; Chen, C.; Wu, H.; Peng, S.; Wang, X.; Dong, L. Quantitative FTIR study of PHBV/bisphenol A blends. *Eur. Polym. J.* **2003**, *39*, 1939−1946.
(34) Hameed, N.; Guo, Q.; Tay, F. H.; Kazarian, S. G. Blends of cellulose and poly(3-hydroxybutyrate-co-3-hydroxyvalerate) prepared from the ionic liquid 1-butyl-3-methylimidazolium chloride. *Carbohydr. Polym.* **2011**, *86*, 94−104.
(35) Chen, T. K.; Tien, Y. I.; Wei, K. H. S. Synthesis and characterization of novel segmented polyurethane/clay nanocomposite via poly(ε-caprolactone)/clay. *J. Polym. Sci., Polym. Chem.* **1999**, *37*, 2225−2233.
(36) Ublekov, F.; Baldrian, J.; Nedkov, E. Crystalline β-structure of PHBV grown epitaxially on silicate layers of MMT. *J. Polym. Sci., Polym. Phys.* **2009**, *47*, 751−755.
(37) Siqueira, G.; Bras, J.; Dufresne, A. Cellulose whiskers versus microfibrils: Influence of the nature of the nanoparticle and its surface functionalization on the thermal and mechanical properties of nanocomposites. *Biomacromolecules* **2009**, *10*, 425−432.
(38) Debenedetti, P. G.; Stillinger, F. H. Supercooled liquids and the glass transition. *Nature* **2001**, *410*, 259−267.
(39) Lu, H.; Nutt, S. Restricted relaxation in polymer nanocomposites near the glass transition. *Macromolecules* **2003**, *36*, 4010−4016.
(40) Xu, X.; Liu, F.; Jiang, L.; Zhu, J. Y.; Haagenson, D.; Wiesenborn, D. P. Cellulose nanocrystals vs. cellulose nanofibrils: a comparative study on their microstructures and effects as polymer reinforcing agents. *ACS Appl. Mater. Interfaces* **2013**, *5*, 2999−3009.
(41) Masenelli−Varlot, K.; Reynaud, E.; Vigier, G.; Varlet, J. Mechanical properties of clay-reinforced polyamide. *J. Polym. Sci., Polym. Phys.* **2002**, *40*, 272−283.
(42) Paşcu, E. I.; Stokes, J.; McGuinness, G. B. Electrospun composites of PHBV, silk fibroin and nano−hydroxyapatite for bone tissue engineering. *Mater. Sci. Eng. C* **2013**, *33*, 4905−4916.
(43) Chen, Z.; Cheng, S.; Xu, K. Block poly(ester-urethane)s based on poly(3-hydroxybutyrate-co-4-hydroxybutyrate) and poly(3-hydroxy-hexanoate-co-3-hydroxyoctanoate). *Biomaterials* **2009**, *30*, 2219−2230.
(44) Mahmoud, K. A.; Mena, J. A.; Male, K. B.; Hrapovic, S.; Kamen, A.; Luong, H. T. J. Electrospun composites of PHBV, silk fibroin and nano-hydroxyapatite for bone tissue engineering. *ACS Appl. Mater. Interfaces* **2010**, *2*, 2924−2932.